



# Development of All-Solid-State Lithium Metal Batteries Using Polymer Electrolytes Based on Polycarbonate Copolymer with Spiroacetal Rings

Shuto Ishii, Kento Kimura, and Yoichi Tominaga\*

All-solid-state lithium metal batteries (ASSLMBs) using lithium as anode are candidates for safe and high energy batteries. Lithium metal is an ideal anode because of its high theoretical storage capacity and low standard electrode potential, but nonuniform Li deposition induces short circuits and safety issues. The development of ASSLMBs having stable charge and discharge cycles remains a challenge. ASSLMB-type cells based on the *branch-P*(DMC/TEG/SPG) electrolyte is demonstrated using LiFePO<sub>4</sub> cathode and Li anode provide stable battery performance. *branch-P*(DMC/TEG/SPG) is a polycarbonate-based copolymer with poly(decamethylene carbonate) [P(DMC)], pentaerythritol (PE), triethylene glycol (TEG), 3,9-bis(1,1-dimethyl-2-hydroxyethyl)-2,4,8,10-tetraoxaspiro[5.5]undecane (spiroglycol, SPG). Solid

polymer electrolyte (SPE) based on this polymer exhibits electrochemically and mechanically stability, as it is reported previously. Cells with the *branch-P*(DMC/TEG/SPG) electrolyte have good discharge capacities at 125, 126, and 106 mAh g<sup>-1</sup> with high coulombic efficiency (>99%) after the 30th cycle of at 0.01, 0.05 and 0.1 C, respectively. X-ray photoemission spectroscopy analysis shows that a moderately thick and LiF-rich cathode electrolyte interphase (CEI) gives rise to stable battery performance. The *branch-P*(DMC/TEG/SPG) electrolyte having viscoelastic nature and high concentration of Li-salt forms the stable CEI. These results further the development of ASSLMBs with long-life and stable performance.

## 1. Introduction

With the growth of demand for electric vehicles, lithium-ion batteries (LiBs) are needed with safer and higher energy density.<sup>[1–6]</sup> The energy density can be improved by increasing the operating voltage and using high-capacity electrode materials.<sup>[7,8]</sup> Lithium metal is an ideal high-capacity anode material because it has high theoretical storage capacity (3860 mAh g<sup>-1</sup>, ten times greater than graphite) and low standard electrode potential (−3.04 V vs. SHE).<sup>[9–13]</sup> Unfortunately, large-scale practical use of lithium metal batteries (LMBs) with conventional organic liquid electrolytes is limited by dendrite growth on the lithium metal anode. Dendrites are brittle and easily detach from lithium anodes, resulting in a rapid loss of capacity and coulombic efficiency (CE).<sup>[14–17]</sup> Dendrites that reach the cathode can also cause

serious problems, including short circuits, thermal runaway, and ignition of the electrolyte.<sup>[18–20]</sup> Suppression of dendrite formation and growth is a priority for LMBs. Uniformity of the electric field, lowering the lithium-ion concentration gradient, and mechanical blocking are theoretically effective for suppressing dendrites.<sup>[21,22]</sup> For example, single-cluster Au-modified current collector has been shown to suppress dendrite growth by enabling a uniform electric field and lithium deposition.<sup>[23]</sup> In contrast, solid electrolytes (SEs) can be used in combination with lithium metal foil, and their moderate mechanical strength is expected to suppress dendrite growth. Consequently, all-solid-state lithium metal batteries (ASSLMBs) using SEs without organic liquid are under development in order to achieve safety and stable battery cycles.<sup>[24–26]</sup> SEs are classified largely into inorganic electrolytes and solid polymer electrolytes (SPEs). Inorganic electrolytes reportedly have good conductivity, although high pressure in battery cells is usually needed because of interface resistance due to their hardness.<sup>[27,28]</sup> In contrast, SPEs are considered to be good possible SEs because of their flexibility and consequent interfacial contact, allowing variable design.<sup>[29,30]</sup> Poly(ethylene oxide) (PEO) has been closely studied as an SPE.<sup>[29,31,32]</sup> PEO can dissolve various Li salts and transport Li<sup>+</sup> ions via the flexible oxyethylene chain.<sup>[33,34]</sup> Unfortunately, PEO-type SPEs have low ionic conductivity ( $10^{-7}$ – $10^{-8}$  S cm<sup>-1</sup> at room temperature) because of their crystallinity, and melting temperature of about 65 °C, and a strong complex formed by Li<sup>+</sup> as  $T_g$  increases.<sup>[33,35–37]</sup> Furthermore, PEO-type SPEs may oxidize at around 3.9 V (vs. Li/Li<sup>+</sup>), causing interface problems on the cathode surface, including unstable cycle performances.<sup>[38–41]</sup> Good interface compatibility, mechanical stability, ionic

S. Ishii, Y. Tominaga

Graduate School of Bio-Applications and Systems Engineering  
Tokyo University of Agriculture and Technology  
2-24-16 Naka-cho, Koganei, Tokyo 184-8588, Japan  
E-mail: ytominag@cc.tuat.ac.jp

S. Ishii  
Technology Development Department  
Teijin Limited  
77 Kitayoshida, Matsuyama, Ehime 791-8530, Japan

K. Kimura, Y. Tominaga  
Department of Applied Chemistry  
Graduate School of Engineering  
Tokyo University of Agriculture and Technology  
2-24-16 Naka-cho, Koganei, Tokyo 184-8588, Japan

Supporting information for this article is available on the WWW under <https://doi.org/10.1002/batt.202500237>

conductivity ( $>10^{-4}$  S cm $^{-1}$ ), and electrochemical stability ( $>4$  V vs. Li/Li $^{+}$ ) are all required in the practical development of SPEs for ASSLMBs.<sup>[29,30,42–44]</sup>

Polycarbonates such as poly(ethylene carbonate) (PEC), poly(propylene carbonate) (PPC), and poly(decamethylene carbonate) (P(DMC)) have won attention as alternative polymer matrices to PEO.<sup>[8,45–51]</sup> PEC-type SPEs are well adapted to ASSLMBs because of their amorphous nature and higher lithium transference numbers ( $>0.5$ ) than for PEO-type SPEs. Unlike PEO, the PEC-type SPE with high Li-salt concentration has low  $T_g$  and high oxidative stability ( $>5$  V vs. Li/Li $^{+}$ ).<sup>[52,53]</sup> ASSLMBs with cross-linked ethylene carbonate-based copolymer having increased modulus have been reported as a long-life battery with more than 400 cycles.<sup>[54]</sup> The discharge capacity was restricted at around 80 mAh g $^{-1}$ , because of poor contact between electrolyte and electrode. Good adhesion appears to be an important property for developing ASSLMBs with stable cycling and high capacity. We recently reported that SPE based on *branch-P*(DMC/TEG/SPG) with 60 wt% LiTFSI was superior to original P(DMC) (Figure 1).<sup>[55]</sup> *branch-P*(DMC/TEG/SPG) is a polycarbonate-based copolymer designed to give good electrochemical and mechanical properties to the electrolyte. Decanediol, with a long aliphatic molecular chain, gives low  $T_g$  and relatively high ionic conductivity of the electrolyte. Pentaerythritol (PE), with a four-branched structure, increases the viscoelastic modulus and Li $^{+}$  conductivity of the electrolyte. Triethylene glycol (TEG), with its oxyethylene chain, promotes the transport of Li $^{+}$  by cooperating with the molecular motion. Spiroglycol (SPG), having rigid and bulky spiroacetal rings, provides amorphous properties for the polymer and increases the viscoelastic modulus and adhesive strength of the electrolyte. The concentration of each monomer is carefully chosen to allow efficient coordination between the individual molecules. For example, the concentration of PE is low in order to prevent insolubility in the process solvent (e.g., tetrahydrofuran) due to excessive branching, and the concentration of TEG is  $<20$  mol% to prevent the formation of strong complex of ether with Li $^{+}$ . Furthermore, these monomers are copolymerized following polymerizing P(DMC) oligomer so as to enhance the ionic conductivity and the mechanical stability by forming a structure with relatively large branching intervals. The optimally designed *branch-P*(DMC/TEG/SPG) exhibits different structural and physical properties from P(DMC). P(DMC) ( $M_w = 3.6 \times 10^4$ ,  $M_w/M_n = 2.0$ ) is a highly crystalline polymer with  $T_m = 57$  °C, whereas *branch-P*(DMC/TEG/SPG) ( $M_w = 2.9 \times 10^4$ ,  $M_w/M_n = 2.0$ ) is an amorphous polymer having no melting point with  $T_g = -15$  °C. *branch-P*(DMC/TEG/SPG) has a moderately branched structure because the Zimm branching factor ( $g'$ ) is 0.95. The storage modulus ( $G'$ ) and loss modulus ( $G''$ ) of *branch-P*(DMC/TEG/SPG) are more than 100 times greater than those of P(DMC) at 60 °C ( $G' = 20\,328$  vs. 132 kPa,  $G'' = 3824$  vs. 29 kPa). The superior

characteristics of *branch-P*(DMC/TEG/SPG) provide good electrochemical and mechanical properties with thermally stable LiTFSI incorporated at a high concentration of 60 wt%. The *branch-P*(DMC/TEG/SPG) electrolyte with 60 wt% LiTFSI has greater adhesive strength (8.0 vs. 1.8 N), ionic conductivity ( $7.4 \times 10^{-6}$  vs.  $1.6 \times 10^{-6}$  S cm $^{-1}$ ), oxidative stability (5.0 vs. 4.6 V), and viscoelasticity ( $G' = 287$  vs. 65 kPa,  $G'' = 263$  vs. 58 kPa) than the P(DMC) electrolyte at room temperature. The heat resistances (5% weight loss temperature:  $T_{ds}$ ) of the P(DMC) and *branch-P*(DMC/TEG/SPG) electrolytes both exceed 260 °C. As the temperature increases, moreover, these electrolytes become more viscous and the ionic conductivity increases. The *branch-P*(DMC/TEG/SPG) electrolyte has greater ionic conductivity ( $7.2 \times 10^{-5}$  vs.  $1.3 \times 10^{-5}$  S cm $^{-1}$ ), and viscoelasticity ( $G' = 38$  vs. 10 kPa,  $G'' = 67$  vs. 20 kPa) than the P(DMC) electrolyte at 60 °C. This superior copolymer electrolyte appears to be suitable for ASSLMBs because it is expected to adhere closely to the electrode, suppress dendrite growth, and withstand repeated charge and discharge cycles.

Below, we report ASSLMBs based on the *branch-P*(DMC/TEG/SPG) electrolyte, using lithium as anode and LiFePO<sub>4</sub> (LFP) as the cathode material. P(DMC) electrolyte was used for comparison. Charge and discharge cycle performances were tested at 0.01, 0.05, and 0.1 C below 60 °C. The evolution of cell resistance and cathode materials upon cycling at 0.05 C was also analyzed by electrochemical impedance spectroscopy (EIS) and by X-Ray photoemission spectroscopy (XPS) combined with scanning electron microscope (SEM) observation, respectively. Results reveal that ASSLMBs with *branch-P*(DMC/TEG/SPG) can be cycled stably with a cathode electrolyte interphase (CEI) layer of adequate thickness and concentration of LiF formed on the LFP cathode. The *branch-P*(DMC/TEG/SPG) electrolyte having viscoelastic nature and a high concentration of Li-salt forms the stable CEI.

## 2. Results and Discussion

### 2.1. Electrochemical Stability and Lithium Transference Numbers ( $t_+$ ) of the P(DMC) and *Branch-P*(DMC/TEG/SPG) Electrolytes

Prior to battery performance tests, we evaluated the electrochemical stability of the P(DMC) and *branch-P*(DMC/TEG/SPG) electrolytes with 60 wt% LiTFSI at 60 °C. Figure 2a,c show cyclic voltammetry (CV) from the open-circuit voltage (OCV) to  $-0.5$  V versus Li/Li $^{+}$ .

In both electrolytes, slight reduction peaks were observed at around 1.5 V in the 1st cycle, but no such peaks were observed

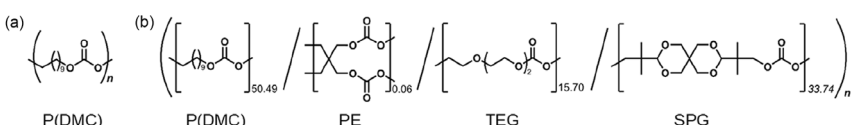
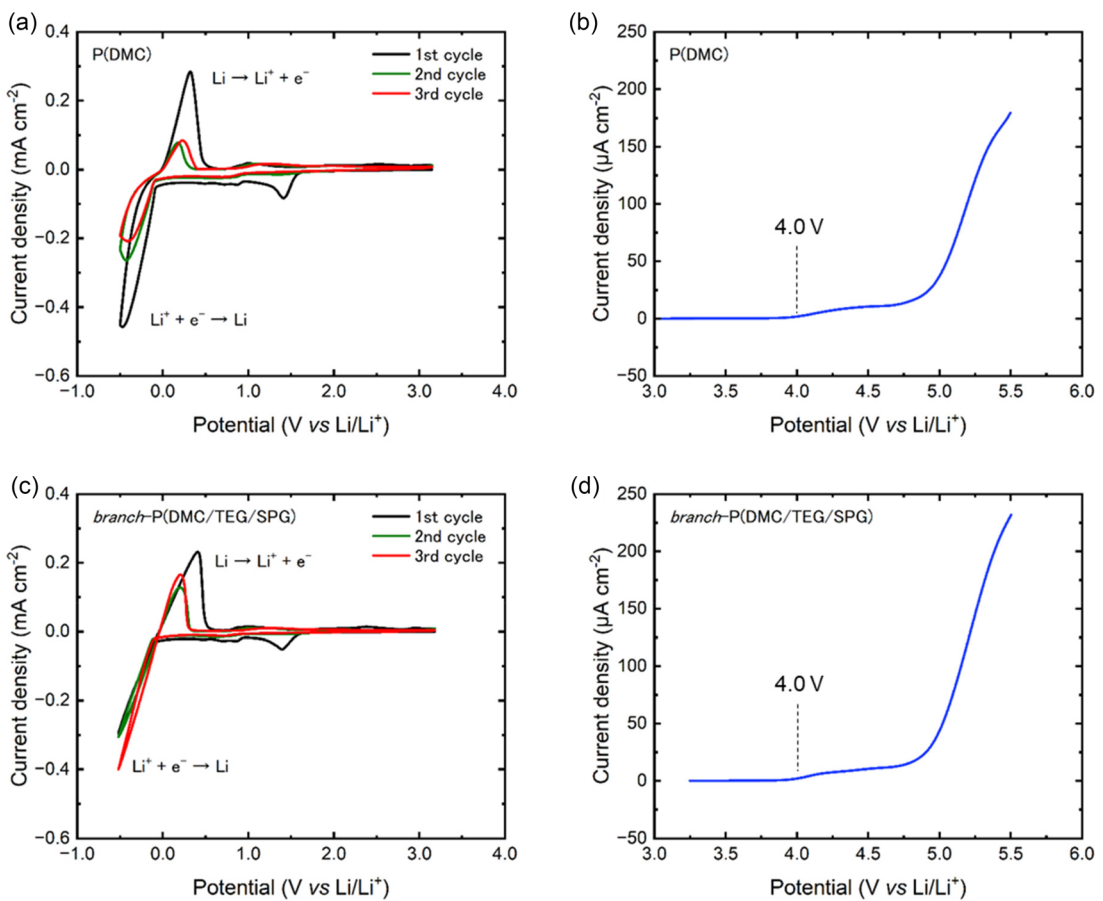


Figure 1. Chemical structures of a) P(DMC) and b) *branch-P*(DMC/TEG/SPG).



**Figure 2.** Cyclic voltammograms (left) from OCV to  $-0.5$  V versus Li/Li<sup>+</sup> and linear sweep voltammograms (right) from OCV to  $5.5$  V versus Li/Li<sup>+</sup> using a Li/SPE/SUS cell at a scan rate of  $1\text{ mV s}^{-1}$  and  $60^\circ\text{C}$ . a,b) P(DMC) with 60 wt% LiTFSI and c,d) branch-P(DMC/TEG/SPG) with 60 wt% LiTFSI.

in later cycles. These peaks may be due to decomposition of polymers or TFSI anion; this decomposition is believed to be related to the formation of solid electrolyte interface (SEI) between the electrolyte and lithium metal surface.<sup>[20]</sup> Reductive and oxidative currents were observed near to 0 V, which correspond to the lithium plating and stripping. In both electrolytes the current decreased with each cycle, but decrease was smaller in the branch-P(DMC/TEG/SPG) electrolyte. We suggest that the stable SEI is formed between the branch-P(DMC/TEG/SPG) electrolyte and the lithium metal, effectively suppressing degradation of the electrolyte. Because the lithium plating and stripping are reversible in both electrolytes, we determined that the reduction limit of both electrolytes is 0 V. Figure 2b,d shows the linear sweep voltammetry (LSV) from OCV to  $5.5$  V. Both electrolytes exhibited a relatively low oxidative current density of  $2\text{ }\mu\text{A cm}^{-2}$  at  $4.0$  V and a high oxidative current density of more than  $4.9$  V. These electrolytes are stable to at least  $4.5$  V at  $30^\circ\text{C}$ , so the increase in temperature to  $60^\circ\text{C}$  seems to have slightly accelerated the oxidative decomposition.<sup>[55]</sup> To repeated charge and discharge cycles in the battery, we determined that the oxidation limit of both electrolytes is  $4.0$  V. These results indicate that both electrolytes are suitable for ASSLB-type batteries with lithium metal and LFP, which typically operates below  $3.8$  V.

Values of  $t_+$  for the P(DMC) and branch-P(DMC/TEG/SPG) electrolytes with 60 wt% of LiTFSI at  $60^\circ\text{C}$  were estimated by electrochemical measurement combined with direct current (DC) polarization and AC impedance methods using a symmetrical Li/SPE/Li coin cell.

Figure 3 shows the results of chronoamperometry and the Nyquist plots by EIS; the data are summarized in Table 1. All plots from EIS measurements were fitted with an equivalent circuit model illustrated in Figure S1, Supporting Information. The  $t_+$  values of the P(DMC) and branch-P(DMC/TEG/SPG) electrolytes were 0.58 and 0.55, respectively. The slight decrease in the  $t_+$  value of the branch-P(DMC/TEG/SPG) electrolyte may be caused by coordination between Li<sup>+</sup> and the oxygen of the ether unit in TEG or the acetal unit in SPG. These values are higher than those of typical PEO electrolyte ( $<0.4$ ).<sup>[37]</sup> The high lithium transference numbers of the electrolyte is believed to contribute to stable lithium plating and stripping and improvement of the battery life. The increase in the interfacial resistance before and after polarization was smaller in the branch-P(DMC/TEG/SPG) electrolyte than in the P(DMC) electrolyte. This indicates that the interface between the branch-P(DMC/TEG/SPG) electrolyte and lithium is stable. Since the relatively high lithium transference numbers and the stable interface may enable stable cycle performance in ASSLMB, we evaluate the battery performance with both electrolytes in the next chapter.

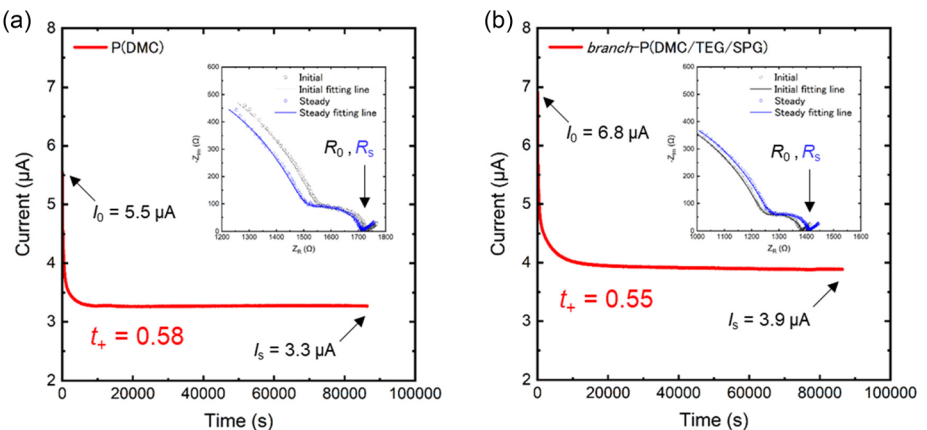


**Figure 3.** Chronoamperograms (DC voltage: 10 mV) and Nyquist plots acquired before and after polarization (insert) for Li/SPE/Li cells at 60 °C for a) P(DMC) with 60 wt% LiTFSI and b) branch-P(DMC/TEG/SPG) with 60 wt% LiTFSI.

Table 1. DC ( $I_0$ , $I_s$ ), Li/electrolyte interfacial resistance ( $R_0$ , $R_s$ ) and lithium transference numbers ( $t_+$ ) using Equation (1) for Li/SPE/Li cells at 60 °C.					
Electrolyte	$I_0$ [ $\mu\text{A}$ ]	$I_s$ [ $\mu\text{A}$ ]	$R_0$ [ $\Omega$ ]	$R_s$ [ $\Omega$ ]	$t_+$
P(DMC) with 60 wt% LiTFSI	5.5	3.3	195	221	0.58
branch-P(DMC/TEG/SPG) with 60 wt% LiTFSI	6.8	3.9	138	142	0.55

## 2.2. Battery Performance

Cycle performance of the ASSLMB-type battery cells with the two different polymers, P(DMC) and *branch*-P(DMC/TEG/SPG), were examined using a constant-current charge/discharge test at 0.01, 0.05, and 0.1 C and 60 °C in the voltage range from 2.5 to 3.8 V. Every cell consists of LiFePO<sub>4</sub> (LFP) cathode, SPE with 60 wt% LiTFSI, and Li metal anode. The LFP cathode is composed of 85 wt% LFP as active material, 5 wt% acetylene black as conductive additive, and 10 wt% PVDF as binder. Figure 4 shows the charge/discharge voltage profiles at 0.01 C. The cell with P(DMC) electrolyte was capable of 30 charge/discharge cycles (Figure 4a, b). The discharge capacity and CE at the 1st cycle were 137 mAh g<sup>-1</sup> and 88.8%, increasing to 139 mAh g<sup>-1</sup> and 98.8% at the 2nd cycle. In the case of liquid LiBs, low CE is a normal behavior in the initial cycles, in which a stable layer is formed between the electrolyte and the electrode.<sup>[56]</sup> Similarly, the low CE in the initial cycle observed in the cell with P(DMC) electrolyte is indicative of the formation of the stable layer at the electrode-electrolyte interface. However, subsequent cycles were unstable in the cell with P(DMC) electrolyte. The discharge capacity started to decrease from the 23rd cycle. The discharge capacity and the CE at the 30th cycle were 130 mAh g<sup>-1</sup> and 97.9%. The significant increase in polarization from the 1st cycle to the 30th cycle suggests that the internal resistance of the cell increased. Electrochemical decomposition of the electrolyte at the electrode interface has been reported to increase the internal resistance of the cell.<sup>[39,57–60]</sup> For the cell with P(DMC), unstable electrode-electrolyte interface might cause continuous electrochemical decomposition of the P(DMC) electrolyte. In contrast, the cell with *branch*-P(DMC/TEG/SPG) electrolyte displayed more stable

battery performance (Figure 4c,d). The discharge capacity and the CE at the 1st cycle were 126 mAh g<sup>-1</sup> and 90.4%, and at the 30th cycle were 125 mAh g<sup>-1</sup> and 100.1%. The increase in the CE from the 1st cycle to the 2nd cycle (90.4–99.0%) is similar to the cell with P(DMC) electrolyte. Unlike the cell with P(DMC) electrolyte, however, the discharge capacity, CE, and the polarization were stable after the 2nd cycle in the cell with *branch*-P(DMC/TEG/SPG) electrolyte. This implies that serious electrochemical decomposition does not occur after the 2nd cycle in the cell with *branch*-P(DMC/TEG/SPG) electrolyte. Clearly a good electrode/electrolyte interface, which inhibits serious electrochemical decomposition, was formed at the 1st cycle in the case of the *branch*-P(DMC/TEG/SPG) electrolyte.

Figure 5 shows the charge/discharge voltage profiles at 0.05 C, where the difference between two polymers is more pronounced. The discharge capacity and the CE of the cell with P(DMC) electrolyte at the 1st cycle were 63 mAh g<sup>-1</sup> and 90.0% (Figure 5a,b). The discharge capacity was less than half that at 0.01 C. The CE fluctuated during the initial 9 cycles before it stabilized from the 10th to the 30th cycle at around 99%. The discharge capacity increased gradually with the stabilized CE. The discharge capacity and the CE at the 30th cycle were 81 mAh g<sup>-1</sup> and 97.9%. The cell with *branch*-P(DMC/TEG/SPG) electrolyte gave better battery performance (Figure 5c,d). The discharge capacity and the CE at the 1st cycle were 128 mAh g<sup>-1</sup> and 89.3%, and at the 30th cycle were 126 mAh g<sup>-1</sup> and 99.9%. The CE gradually increased from the 1st to the 4th cycle and reached about 99% at the 5th cycle. Thereafter, the CE was stable until the 30th cycle. In contrast to the cell with P(DMC) electrolyte, the 30th discharge capacity of the cell with *branch*-P(DMC/TEG/SPG) electrolyte at 0.01 and 0.05 C were almost the same (125 vs. 126 mAh g<sup>-1</sup>). Although the charge/discharge rate was increased fivefold, no significant electrochemical decomposition was apparent at the cell with *branch*-P(DMC/TEG/SPG) electrolyte. A smaller number of cycles were required for stabilization in the cell with *branch*-P(DMC/TEG/SPG) electrolyte than in the cell with P(DMC) electrolyte. Polar monomer units such as TEG and SPG copolymerized with *branch*-P(DMC/TEG/SPG) apparently influences the formation

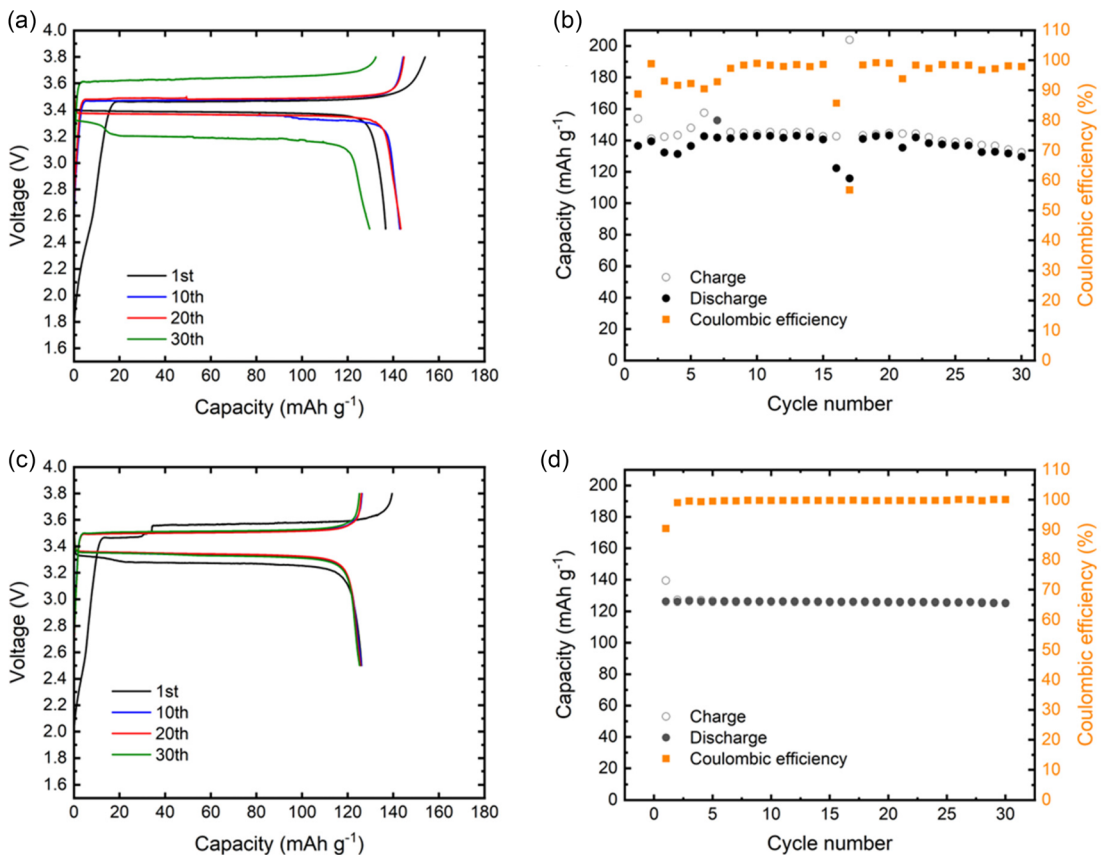


**Figure 4.** Charge/discharge voltage profiles (left) and cycling performance (right) of Li/electrolyte/LFP cells at 0.01 C (1C = 170 mA g<sup>-1</sup>) and 60 °C. a,b) P(DMC) with 60 wt% LiTFSI (cathode mass loading: 4.7 mg cm<sup>-2</sup>, active mass loading: 4.0 mg cm<sup>-2</sup>, cathode thickness: 46 µm, estimated electrolyte thickness: 214 µm) and c,d) branch-P(DMC/TEG/SPG) with 60 wt% LiTFSI (cathode mass loading: 2.6 mg cm<sup>-2</sup>, active mass loading: 2.2 mg cm<sup>-2</sup>, cathode thickness: 27 µm, estimated electrolyte thickness: 233 µm).

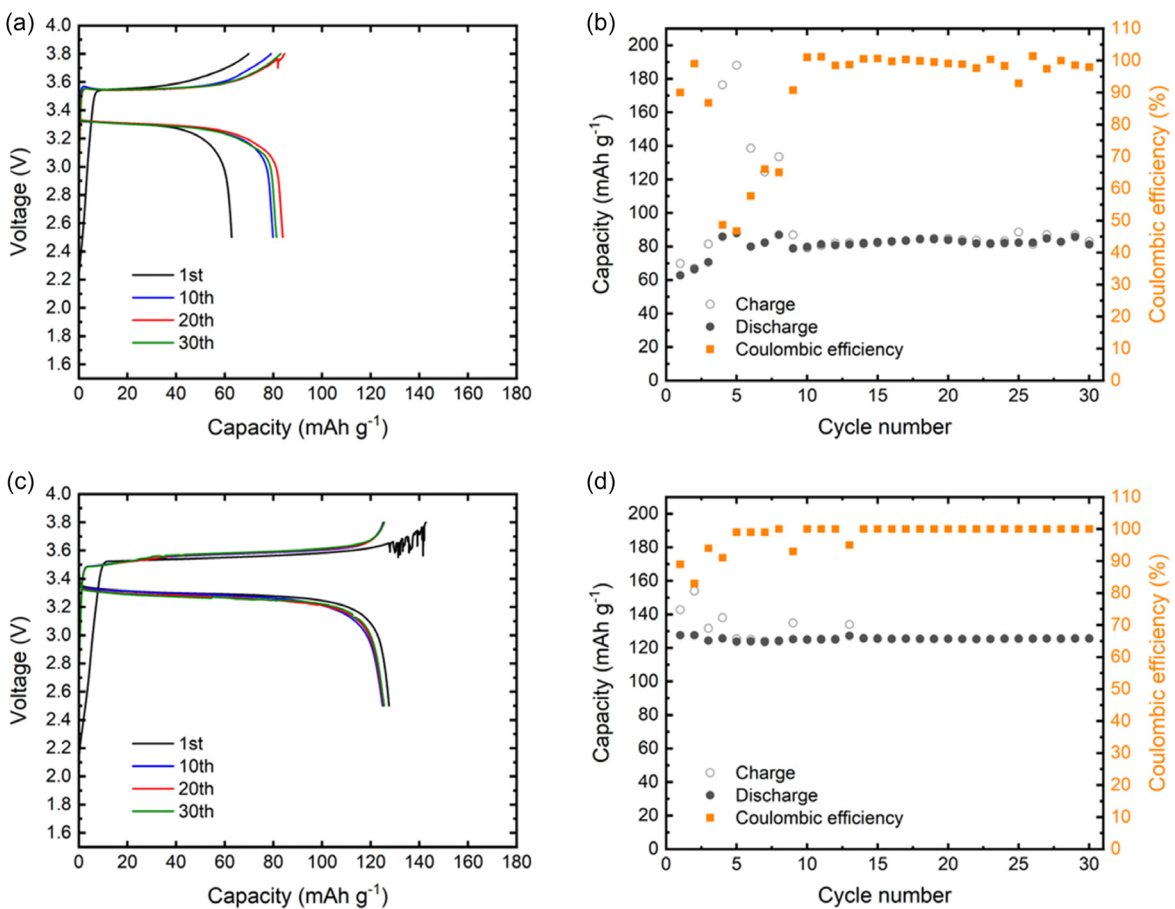
of a good interface between the electrolyte and the electrode. To identify the mechanism, further analysis will be conducted in later chapters.

Figure 6 shows the charge/discharge voltage profiles at 0.1 C, for which clear differences are visible between the two polymer electrolytes. The cell with P(DMC) electrolyte had a discharge capacity of 36 mAh g<sup>-1</sup> at the 1st cycle, although this decreased suddenly to 1 mAh g<sup>-1</sup> at the 15th cycle (Figure 6a,b). Since the cell began to show overcharging behavior at the 8th cycle, an internal short circuit was suspected. In contrast, the cell with branch-P(DMC/TEG/SPG) electrolyte was charged and discharged stably at the 30th cycle with no short circuit (Figure 6c,d). The discharge capacity and the CE at the 1st cycle were 126 mAh g<sup>-1</sup> and 79.9%, and at the 30th cycle were 106 mAh g<sup>-1</sup> and 99.9%. As seen in 0.05 C, the CE at 0.1 C increased gradually from the 1st to the 4th cycle and was above 99% from the 5th to the 30th cycle. The 1st cycle discharge capacity was similar to those at 0.01 and 0.05 C. The discharge capacity gradually decreased, but was still 84% after the 30th cycle. A sudden drop of the discharge capacity in the cell with P(DMC) electrolyte has been reported in SPEs with poor mechanical stability.<sup>[20,40,54,61]</sup> The storage modulus ( $G'$ ) and  $\tan \delta$  ( $=G''/G'$ ) values at 60 °C for the branch-P(DMC/TEG/SPG) electrolyte are about 38 kPa and 1.8, and for the P(DMC) electrolyte are 10 kPa and 2.0.<sup>[55]</sup> The  $G'$  value of the PVA electrolyte, which is a typical gel

electrolytes, is 3 kPa, and the  $\tan \delta$  value is  $<1.0$  at room temperature.<sup>[62]</sup> Since the  $G'$  value of the P(DMC) electrolyte at 60 °C is close to that of a gel electrolyte, it appears to be mechanically unstable. Thus, the P(DMC) electrolyte might detach partially from the electrode during charge/discharge cycles and cause unstable cycle performance. In contrast, the branch-P(DMC/TEG/SPG) electrolyte has about ten times greater  $G'$  value than the gel electrolyte and has the relatively high  $\tan \delta$  value. It follows that the branch-P(DMC/TEG/SPG) electrolyte maintained its form as a solid electrolyte yet adhered flexibly to the electrode. We suppose that the branch-P(DMC/TEG/SPG) electrolyte with relatively high  $G'$  value and  $\tan \delta$  value prevents the detachment from the Li anode and LFP cathode.

### 2.3. EIS Analysis of Batteries

To further investigate the internal resistance behavior of the cells for 0.05 C, EIS measurements were performed before the cycling and after the 30th cycle. Figure 7 shows Nyquist plots with fitting curves; the results of the fitting analysis are summarized in Table 2. All plots were fitted with an equivalent circuit model, shown in Figure S2, Supporting Information. In this circuit model,  $R_{SPE}$ ,  $R_{anode}$ , and  $R_{cathode}$  respectively denote the bulk resistance of SPE and the charge-transfer resistance between the Li/SPE interface and LFP/SPE interface;  $W$  is the Warburg impedance.



**Figure 5.** Charge/discharge voltage profiles (left) and cycling performance (right) of Li/electrolyte/LFP cells at 0.05 C and 60 °C. a,b) P(DMC) with 60 wt% LiTFSI (cathode mass loading: 3.3 mg cm<sup>-2</sup>, active mass loading: 2.8 mg cm<sup>-2</sup>, cathode thickness: 33 µm, estimated electrolyte thickness: 227 µm) and c,d) branch-P(DMC/TEG/SPG) with 60 wt% LiTFSI (cathode mass loading: 3.7 mg cm<sup>-2</sup>, active mass loading: 3.1 mg cm<sup>-2</sup>, cathode thickness: 37 µm, estimated electrolyte thickness: 223 µm).

A semicircle at higher frequency ( $\approx 3$  MHz), middle frequency ( $\approx 2$  kHz), and low frequency ( $\approx 70$  Hz) assigned to  $R_{\text{SPE}}$ ,  $R_{\text{anode}}$ , and  $R_{\text{cathode}}$ , respectively<sup>[54,63,64]</sup> For the cell with P(DMC) electrolyte, all resistances increased significantly from before to after cycling. The value of  $R_{\text{SPE}}$  after cycling increased, which implies electrochemical decomposition of the P(DMC) electrolyte. Previous studies of PEO electrolytes have reported that continued decomposition of the polymer leads to the formation of an unstable SEI and CEI.<sup>[38,65]</sup> The unstable SEI induces heterogeneous lithium deposition and dendrite growth on lithium anodes. The unstable CEI causes continuous oxidative decomposition of SPE on the cathode. In fact,  $R_{\text{anode}}$  and  $R_{\text{cathode}}$  values of the cell with P(DMC) electrolyte after cycling were much greater than before cycling. Based on these results, an unstable SEI or CEI appears to cause electrochemical decomposition at the interface of both electrodes and unstable cycling at 0.05 C for the cell with P(DMC) electrolyte.

The increasing trend of the resistance from before and after cycling at 0.05 C of the cell with branch-P(DMC/TEG/SPG) electrolyte was different from the P(DMC) electrolyte. The  $R_{\text{SPE}}$  value was almost the same or was slightly lower after the cycling than before. These results indicate that the branch-P(DMC/TEG/SPG) electrolyte does not decompose like the P(DMC) electrolyte.

Furthermore, the  $R_{\text{anode}}$  values did not increase. These results indicate that the branch-P(DMC/TEG/SPG) electrolyte forms stable SEI on the anode and suppresses the formation of dendrites. The good elastic modulus of the branch-P(DMC/TEG/SPG) electrolyte appears to cause this suppression. In particular, the  $R_{\text{cathode}}$  value increased. Formation of the CEI is generally accompanied by an increase in resistance.<sup>[66]</sup> The stable CEI is believed to form between the LFP cathode and the branch-P(DMC/TEG/SPG) electrolyte. Based on these results, the stable battery performance of the cell with branch-P(DMC/TEG/SPG) is due not only to the suppression of dendrite growth on the anode and decomposition of the electrolyte but also to the formation of the stable CEI on the cathode. To understand the mechanism of stability by the CEI, we analyze the composition of the CEI in the following chapter.

#### 2.4. XPS and Morphology Analysis of Cathodes Before and After Cycling at 0.05 C

To understand the stable battery performance with the branch-P(DMC/TEG/SPG) electrolyte, LFP cathodes were analyzed before and after cycling at 0.05 C. Figure S3, Supporting Information, shows SEM images of the cathode surface. No cracks were visible before or after cycling. Consequently, the increase in the

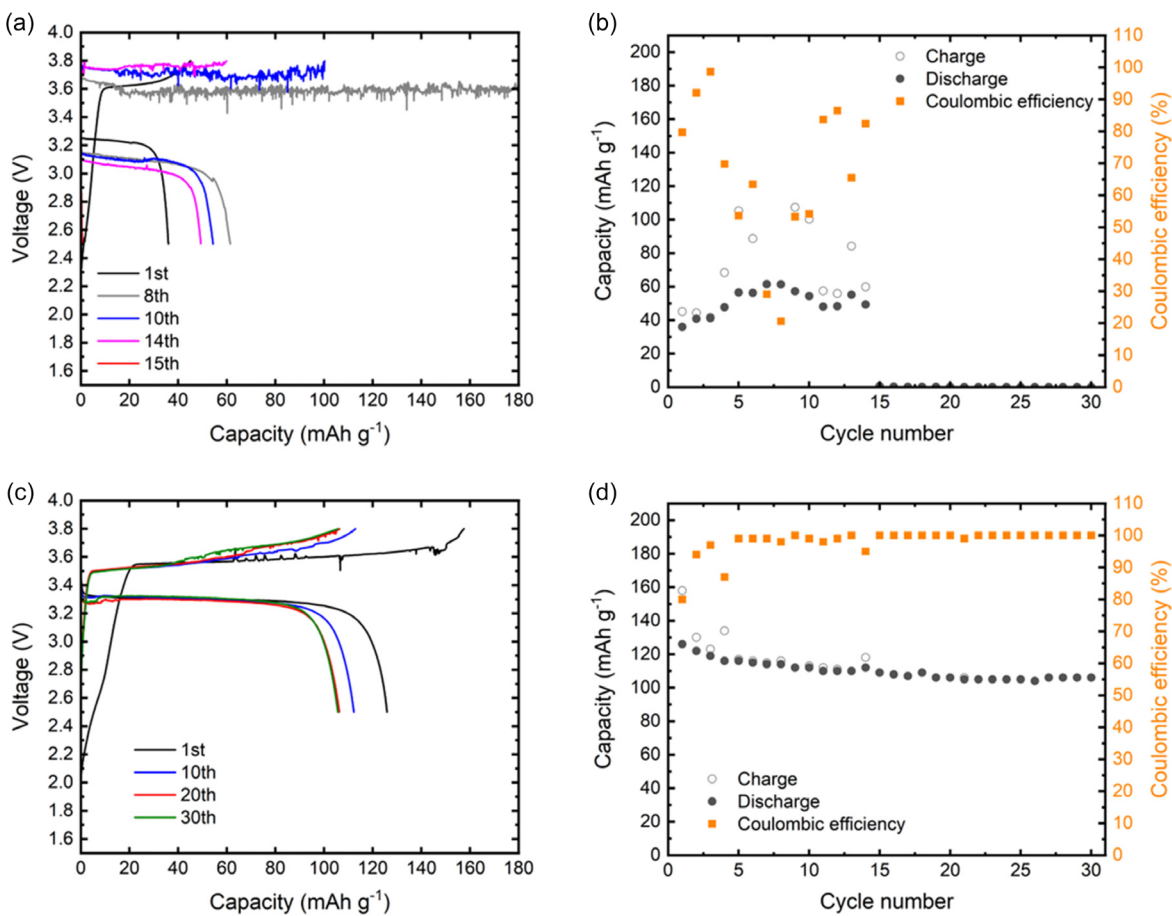


**Figure 6.** Charge/discharge voltage profiles (left) and cycling performance (right) of Li/electrolyte/LFP cells at 0.1 C and 60 °C. a,b) P(DMC) with 60 wt% LiTFSI (cathode mass loading: 3.9 mg cm<sup>-2</sup>, active mass loading: 3.3 mg cm<sup>-2</sup>, cathode thickness: 38 µm, estimated electrolyte thickness: 222 µm) and c,d) branch-P(DMC/TEG/SPG) with 60 wt% LiTFSI (cathode mass loading: 4.2 mg cm<sup>-2</sup>, active mass loading: 3.6 mg cm<sup>-2</sup>, cathode thickness: 41 µm, estimated electrolyte thickness: 219 µm).

resistance of the cathode is not due to cracks. **Figure 8** and S4, Supporting Information, show the results of XPS. The PO<sub>4</sub><sup>3-</sup> bonding of LFP was identified in the fresh cathode (P 2p signal at 133.5 eV).<sup>[56]</sup> The corresponding peak after cycling in both cells was identified using the P(DMC) electrolyte and the branch-P(DMC/TEG/SPG) electrolyte at 133.5 eV, although the intensities were very weak (Figure 8a). In addition, the peaks centered at 532.0 eV for the cell using P(DMC) electrolyte and at 532.4 eV for the cell using branch-P(DMC/TEG/SPG) electrolyte do not correspond to the PO<sub>4</sub><sup>3-</sup> bonding of LFP (O 1s signal at 531.4 eV).<sup>[56]</sup> These peaks at 532.0 and 532.4 eV are assigned to the O-C=O group of lithium carbonate (Li<sub>2</sub>CO<sub>3</sub>) and the C-O-C group of ether (Figure 8b).<sup>[67]</sup> Furthermore, the Fe 2p spectrum of the fresh cathode resembles typical LFP,<sup>[68]</sup> whereas broad and weak spectra were gained from both cells only after cycling (only the spectrum of the fresh cathode is shown in Figure S4a, Supporting Information). These results indicate the change in surface conditions and the presence of CEIs on both cathodes after cycling. The binding energies of the other peaks were almost the same in both two cells. Figure 8c shows the C 1s region of XPS spectra. The peaks at 284.7, 286.4, and 288.7 eV are assigned to the C-C/C-H group, the C-O-C group, and the O-C=O group.<sup>[38,69]</sup> We believe these peaks originate from the polymer that comprises

SPE. In particular, the peak of the C-O-C group for branch-P(DMC/TEG/SPG) may be derived from ether of TEG or acetal of SPG. The peaks at 292.9 eV are assigned to the C-F group derived mainly from LiTFSI. The peaks at 688.4 eV for the C-F group (Figure 8d), 399.5 eV for the N-S group (Figure S4b, Supporting Information), and 169.0 and 170.1 eV for the SO<sub>2</sub>CF<sub>3</sub> group (Figure S4c, Supporting Information) also derive from LiTFSI.<sup>[67,70]</sup> In Figure 8c, the peaks at 290.5 eV are assigned to the O-C=O group derived from Li<sub>2</sub>CO<sub>3</sub>.<sup>[67]</sup> We suppose that Li<sub>2</sub>CO<sub>3</sub>, which is thermodynamically unstable, was produced by the decomposition of LiTFSI and the organic polymer electrolyte.<sup>[67,71,72]</sup> Peaks from the decomposition products of LiTFSI were also detected at 167.1 and 168.2 eV, although the detailed structure is not known (Figure S4c, Supporting Information).<sup>[70,73-75]</sup> Figure 8d shows the presence of LiF in the CEI for both cells after cycling (F 1s signal at 685.0 eV). LiF is a stable inorganic compound that enhances the stability of the CEI.<sup>[66,76]</sup> Figure S4d, Supporting Information, shows the peak derived from LiF at 55.5 eV; this peak is difficult to separate from the other peaks derived from LiTFSI and Li<sub>2</sub>CO<sub>3</sub>.<sup>[67,77]</sup>

Table S1 and S2, Supporting Information, list the respective atomic concentrations (at%) of all cathodes. Compared with the fresh cathode, both cathodes show much lower phosphorus

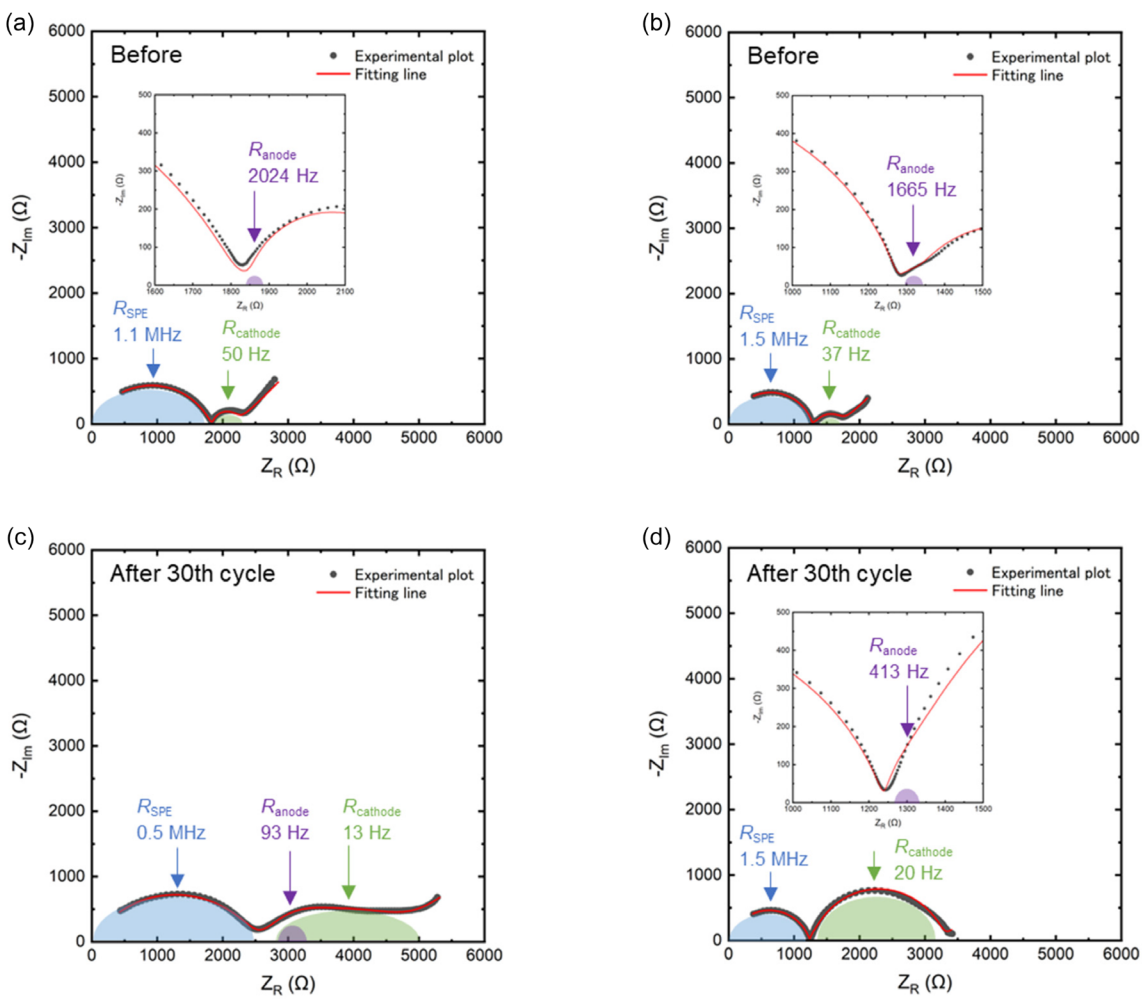


**Figure 7.** Nyquist plots of Li/electrolyte/LFP cells with P(DMC) electrolyte (left) and *branch*-P(TEG/SPG) electrolyte (right). a,b) before cycling and c,d) after cycling at 0.05 C.

Electrolyte in Li/LFP cell	$R_{\text{SPE}}$ [Ω]	$R_{\text{anode}}$ [Ω]	$R_{\text{cathode}}$ [Ω]
Before cycle with P(DMC)	1820	38	366
After 30th cycle with P(DMC)	2500	269	2274
Before cycle with <i>branch</i> -P(TEG/SPG)	1280	45	418
After 30th cycle with <i>branch</i> -P(TEG/SPG)	1240	55	1978

atomic concentration derived from LFP after cycling. We believe that the decrease in the atomic concentrations of phosphorus in the cathode after cycling is due to the formation of CEI on the cathode. The phosphorus atomic concentration for the fresh cathode is 4.6 at%, for the cathode with P(DMC) electrolyte is 1.0 at%, and with *branch*-P(TEG/SPG) electrolyte is 0.8 at%. These results indicate that the CEIs of both cells cover the LFP cathodes. The CEIs of both cells after cycling contain large amounts of carbon derived from polymer. In particular, the CEI of the cathode with *branch*-P(TEG/SPG) electrolyte contains a higher concentration of carbon derived from ether than the P(DMC)

electrolyte (12.2 vs. 8.9 at%). This indicates that the polar TEG with ether and SPG with acetal, copolymerized in *branch*-P(TEG/SPG), contribute to a strong interaction with the LFP cathode and promote the formation of the CEI. Furthermore, the CEI of the cathode with *branch*-P(TEG/SPG) electrolyte contains a higher concentration of fluorine derived from LiF than the P(DMC) electrolyte (0.8 vs. 0.4 at%). In contrast, the CEI of the cathode with *branch*-P(TEG/SPG) electrolyte contains a lower concentration of carbon derived from  $\text{Li}_2\text{CO}_3$  than the P(DMC) electrolyte (3.7 vs. 5.8 at%). These results indicate that the CEI formed by the *branch*-P(TEG/SPG) electrolyte contains a large amount of stable LiF and a low amount of unstable  $\text{Li}_2\text{CO}_3$ , contributing to stable battery cycling.

To analyze the composition through the depth of the CEI of LFP cathodes after the 30th cycle at 0.05 C, depth analysis by XPS combined with argon sputtering was performed to a distance of 30 nm (the thickness is  $\text{Ta}_2\text{O}_5$  equivalent). **Figure 9**, S5, and Table S3, Supporting Information, show the atomic concentrations corresponding to each functional group as a function of depth. In both cells the atomic concentrations of phosphorus and iron derived from the LFP increased with depth (Figure S5a and Table S3, Supporting Information). This means that the

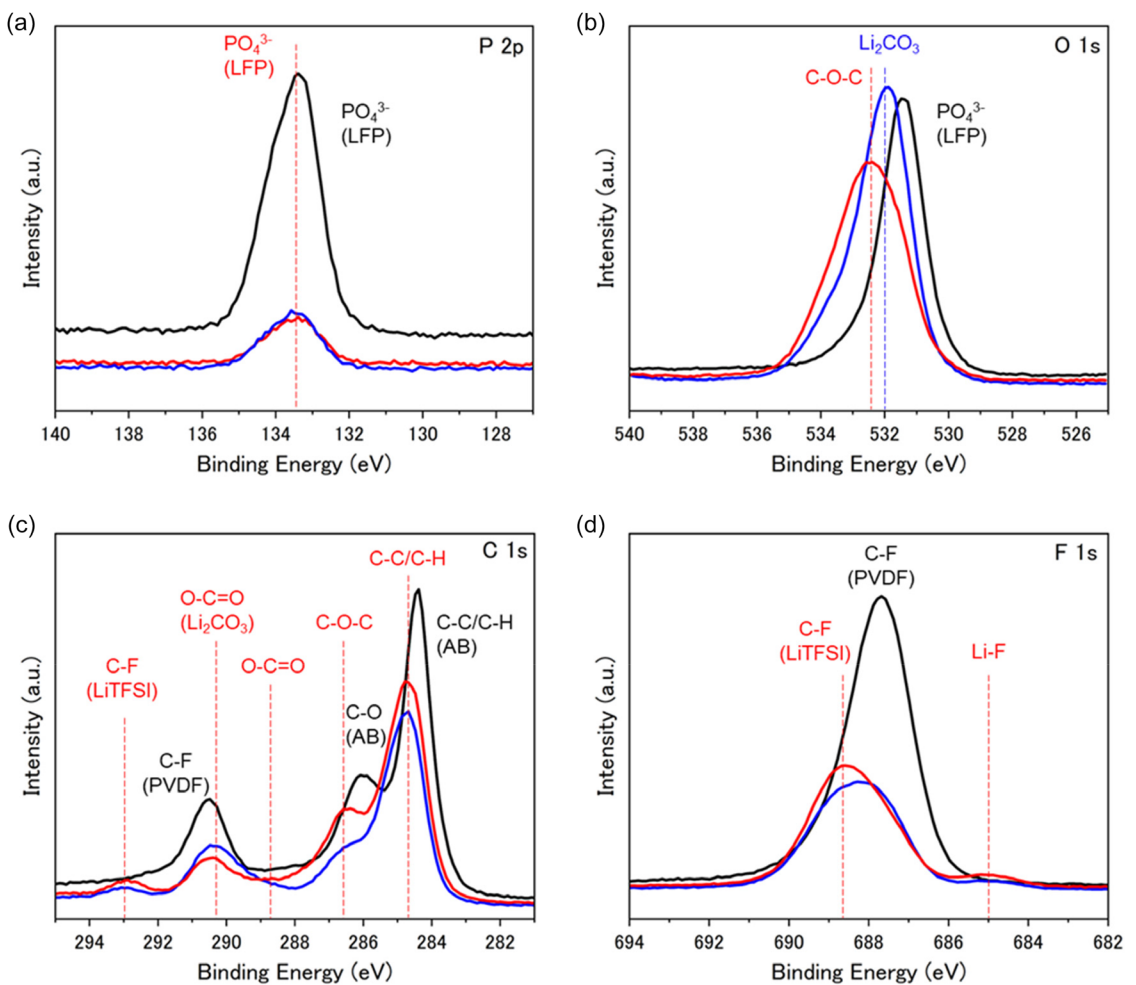


**Figure 8.** Comparison of XPS analyzes for cathode surface among fresh (black line), after 30th cycle with the P(DMC) electrolyte (blue line) and after 30th cycle with the branch-P(DMC/TEG/SPG) electrolyte (red line). Collected XPS spectra of a) P 2p, b) O 1s, c) C 1s, and d) F 1s.

surface of the CEI was scraped off by Ar ion-sputtering, allowing the surface of the LFP cathode to be detected. Since the atomic concentrations of phosphorus and iron at around 30 nm in both cells are lower than those of the fresh cell at the surface, the CEI thickness of both cells may be 30 nm or more. As the concentrations of phosphorus and iron at around 30 nm are lower in the CEI with *branch*-P(DMC/TEG/SPG) electrolyte, we suppose that the CEI formed with the *branch*-P(DMC/TEG/SPG) electrolyte is thicker than that with the P(DMC) electrolyte. Figure 9a and S5b show the atomic concentration of carbon derived from C-C/C-H and C-O-C. The concentrations of the deep region were same as those of the surface region in both cells. This implies that polymers are closely involved in the growth of the CEI. In addition, the concentrations of carbon in the deep region of the CEI for the cell with *branch*-P(DMC/TEG/SPG) are higher than that for the P(DMC) electrolyte. This indicates that the *branch*-P (DMC/TEG/SPG) electrolyte adheres tightly to the LFP cathode and becomes the core for growth of the CEI. The moderate viscosity and polarity of the *branch*-P(DMC/TEG/SPG) electrolyte suppressed detachment from the LFP cathode and promoted the growth of the CEI. Figure 9b shows the atomic concentrations of fluorine derived from LiTFSI. In both cells, the

concentrations of fluorine decreased strongly with depth. This change is greater in the cell with *branch*-P(DMC/TEG/SPG) electrolyte. The decrease in LiTFSI concentrations implies that LiTFSI has changed into another compound close to the LFP surface. Figure 9c shows the atomic concentrations of carbon derived from the  $\text{Li}_2\text{CO}_3$ . In both cells these concentrations in the deep region were same as in the surface region. The CEI of the cell with *branch*-P(DMC/TEG/SPG) electrolyte contains a relatively low concentration of  $\text{Li}_2\text{CO}_3$ . The battery cycle was therefore stable in the cell with *branch*-P(DMC/TEG/SPG) electrolyte. Figure 9d shows the atomic concentration of fluorine derived from LiF. In both cells the concentrations of fluorine from LiF increased strongly with depth. In the two cells, the cell with *branch*-P(DMC/TEG/SPG) electrolyte contains a higher concentration of LiF. We believe that LiF is mostly produced by the LiTFSI.<sup>[67,70,74]</sup> In regard to the decrease in the concentration of LiTFSI at deep region, LiTFSI may be changed to LiF near the LFP surface. The abundant LiF may be due to the high concentration of LiTFSI (60 wt%) in the electrolyte. Based on these results, the large concentration of LiF near the LFP surface suppresses excessive decomposition of the *branch*-P(DMC/TEG/SPG) electrolyte and assists stable battery cycles. The *branch*-P(DMC/TEG/SPG) electrolyte adheres to the LFP

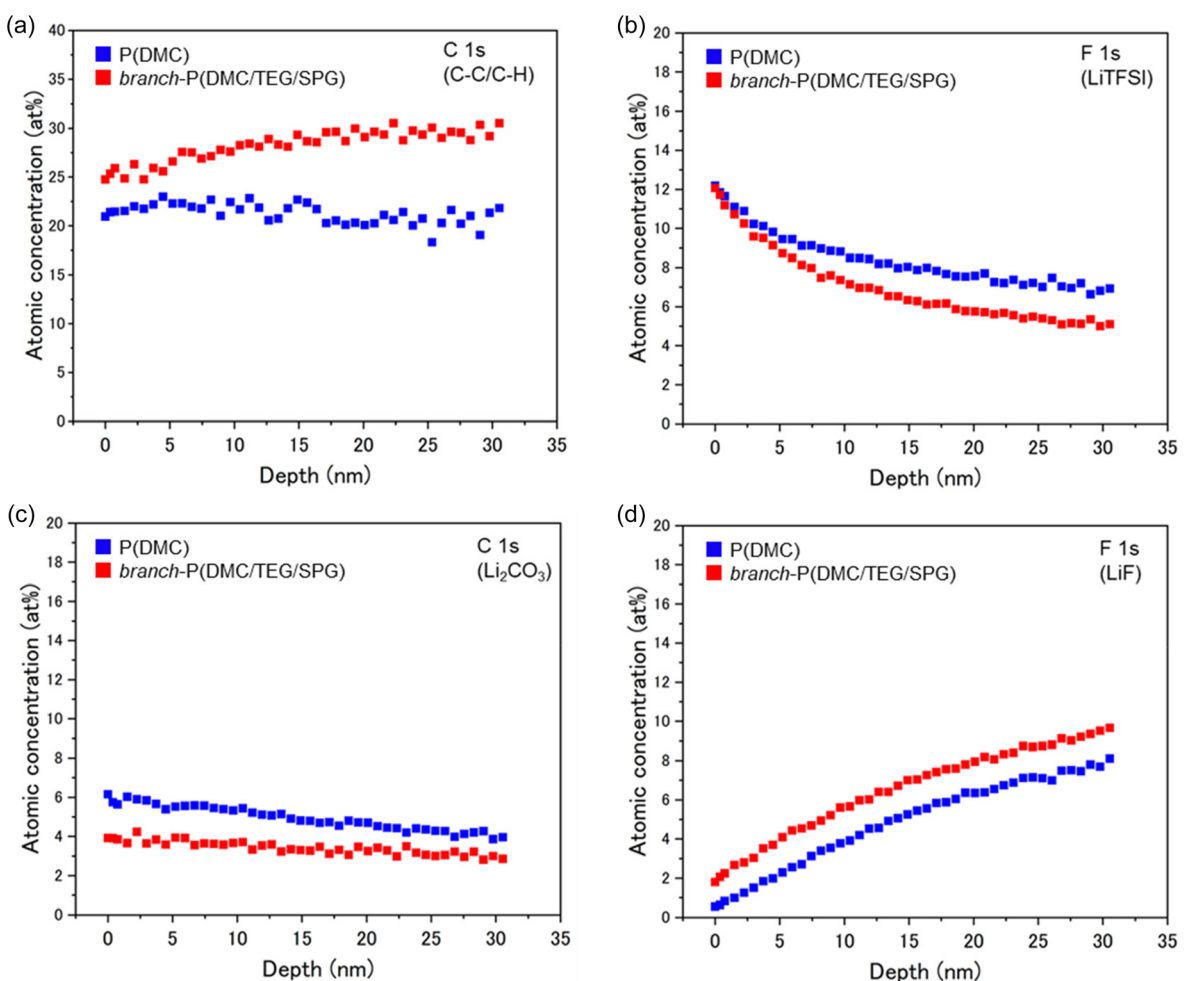


**Figure 9.** Depth profiles of the CEI on LFP cathodes for after 30th cycling at 0.05 C by XPS. a) C-C/C-H (from C 1s signal), b) LiTFSI (from F 1s signal), c) Li<sub>2</sub>CO<sub>3</sub> (from C 1s signal), and d) LiF (from F 1s signal).

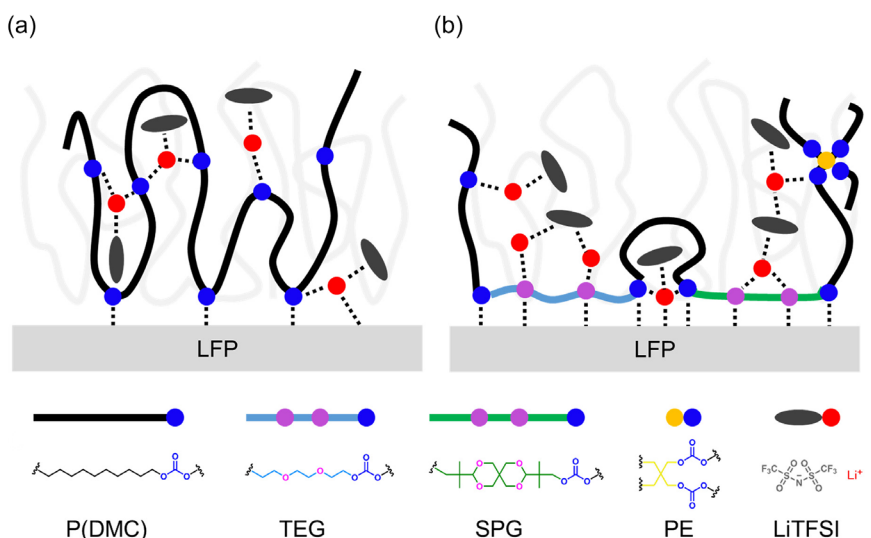


**Figure 10.** Schematic representation of the adhesion of SPEs to the LFP cathode. a) P(TEG/SPG) electrolyte and b) branch-P(TEG/SPG) electrolyte.

surface tightly through the oxygen of ether, acetal, and carbonate and transfers lithium ions and TFSI anions near the LFP surface (**Figure 10**). Close contact between SPE and the LFP cathode leads

to efficient growth of the CEI with LiF. We believe that this thick CEI with LiF is responsible for the stable battery performance of the cell with branch-P(TEG/SPG).

### 3. Conclusion

To develop ASSLMBs with stable battery performance, we studied the electrochemical stability and battery performance at 60 °C of two SPEs with different ionic conductivities and viscoelastic properties. The *branch-P*(DMC/TEG/SPG) and P(DMC) electrolytes with 60 wt% LiTFSI exhibited the identical electrochemical window of 0–4.0 V versus Li/Li<sup>+</sup>, and  $t_+$  values of 0.55 and 0.58, respectively. ASSLMB-type cells based on the *branch-P*(DMC/TEG/SPG) electrolyte using LFP cathode and Li anode exhibited stable battery performance without any short circuit caused by the serious electrochemical decomposition or lithium dendrite. Despite the high temperature (60 °C), discharge capacities after 30th cycle at 0.01, 0.05, and 0.1 C were 125, 126, and 106 mAh g<sup>-1</sup>, with high CE over 99%. EIS results after the 30th cycle at 0.05 C showed little change in the bulk resistance of SPE ( $R_{SPE}$ ), or the charge-transfer resistance between the Li/SPE interface ( $R_{anode}$ ), but an increase in the charge-transfer resistance between the LFP/SPE interface ( $R_{cathode}$ ). XPS results revealed that moderately thick and LiF-rich CEI formed on the LFP cathode in the cells after cycling. In contrast, the cell with P(DMC) exhibited unstable battery performance. Discharge capacities after 30th cycle at 0.01 and 0.05 C were 130 and 81 mAh g<sup>-1</sup>, with CE about 98%. At 0.1 C, the cell with P(DMC) was not able to charge and discharge 30 times because of an internal short circuit at the 15th cycle. EIS results after 30th cycle at 0.05 C showed that all resistances ( $R_{SPE}$ ,  $R_{anode}$ , and  $R_{cathode}$ ) increased significantly from before to after cycling, implying electrochemical decomposition of the P(DMC) electrolyte at both electrode interfaces. XPS results revealed that the CEI included a low concentration of LiF and polymers, and a relatively high concentration of Li<sub>2</sub>CO<sub>3</sub> was formed on the LFP cathode in the cells with P(DMC) electrolyte after cycling. Good battery performance of the cells with the *branch-P*(DMC/TEG/SPG) electrolyte was achieved due to the good mechanical and electrochemical properties of the *branch-P*(DMC/TEG/SPG) electrolyte. Viscoelastic and adhesive properties of the *branch-P*(DMC/TEG/SPG) electrolyte caused close adhesion to both electrodes and suppression of serious electrochemical decomposition or dendrite growth. The *branch-P*(DMC/TEG/SPG) electrolyte with a high concentration of LiTFSI (60 wt%) made close contact with the LFP cathode surface, supporting the efficient growth of the CEI with LiF. These findings contribute positively to the further development of SPEs that will enable long-life and stable ASSLMBs.

### 4. Experimental Section

#### Materials

We used as received the following materials; lithium bis(trifluoromethane sulfonyl)imide (LiTFSI, 99.9% battery grade, Kishida Chemical Co., Japan), tetrahydrofuran (THF, dehydrated, stabilizer-free grade, FUJIFILM Wako Chemicals Co., Japan), LiFePO<sub>4</sub> (LFP, battery grade, MTI Co., USA), poly(vinylidene fluoride) (PVDF,  $M_w = 6.0 \times 10^5$ , battery grade, MTI Co., USA), acetylene black (AB, battery grade, MTI Co., USA), N-methyl pyrrolidone (NMP, dehydrated grade, FUJIFILM Wako Chemicals Co., Japan), glass-fiber type filter paper (260 µm, Whatman GF/A grade, Cytiva Co., Japan), Li metal foil (200 µm, Ø15.5 mm, Honjo Metal Co., Japan), Al foil (20 µm, double-sided

polishing, Hohsen Co., Japan), CR2032 coin cell (stainless steel (SUS), Hohsen Co., Japan). The P(DMC) ( $M_w = 3.6 \times 10^4$ ,  $M_w/M_n = 2.0$ ) and *branch-P*(DMC/TEG/SPG) ( $M_w = 2.9 \times 10^4$ ,  $M_w/M_n = 2.0$ ) used in this work were the same as those polymerized and analyzed in our previous work.<sup>[55]</sup> The concentration of LiTFSI in the electrolyte was chosen as 60 wt%, as this composition exhibited the highest ionic conductivity and good mechanical properties among those investigated. The ionic conductivity and viscoelastic properties of the electrolyte with 60 wt% of LiTFSI at 60 °C are: P(DMC):  $\sigma = 1.3 \times 10^{-5}$  S cm<sup>-1</sup>,  $G' = 10$  kPa,  $G'' = 20$  kPa,  $\tan \delta = 2.0$ , and *branch-P*(DMC/TEG/SPG):  $\sigma = 7.2 \times 10^{-5}$  S cm<sup>-1</sup>,  $G' = 38$  kPa,  $G'' = 67$  kPa,  $\tan \delta = 1.8$ .

#### Preparation of SPE

Prior to the measurement of electrochemical stability and lithium transference numbers ( $t_+$ ), SPE was prepared in an Ar gas-filled glovebox. P(DMC) and *branch-P*(DMC/TEG/SPG) were dried under vacuum at 110 °C for 5 h before use. P(DMC) or *branch-P*(DMC/TEG/SPG) and LiTFSI at a weight ratio of 4:6 were dissolved in THF. The solvent was dried at 65 °C for 12 h under normal pressure and then vacuum dried at 65 °C for 72 h. The resulting SPE was used in the next cell assembly process.

#### Electrochemical Stability of SPE

The electrochemical stability of SPE at 60 °C was determined by CV and LSV, using an SP-50ez (Bio-Logic Co., France). The CR2032-type Li/SPE/SUS cell was assembled by using polypropylene O-ring (Ø16 mm for outer and Ø6 mm for inner, and thickness of 100 µm) to hold the SPE. The SPE was sandwiched between a SUS-disk (Ø15.5 mm) as working electrode and Li metal foil (Ø15.5 mm) as counter electrode. The cell was assembled in an Ar gas-filled glovebox, and the resulting cells were maintained at 60 °C for 24 h. CV was carried out from OCV to -0.5 V three times, and LSV was carried out from OCV to 5.5 V with a scanning rate of 1 mV s<sup>-1</sup> at 60 °C.

#### Lithium transference numbers ( $t_+$ ) of SPE

The lithium transference number ( $t_+$ ) of SPE was estimated by DC polarization and EIS, using an SP-50ez (Bio-Logic Co., France).<sup>[47]</sup> The CR2032-type Li/SPE/Li cell was assembled by using polypropylene O-ring (Ø16 mm for outer and Ø6 mm for inner, and thickness of 100 µm) to hold the SPE, which was sandwiched between Li metal foils (Ø15.5 mm). The cell was assembled in a glovebox filled with Ar gas, and the resulting cells were kept at 60 °C for 24 h in order to stabilize Li/SPE interfacial contact. Chronoamperometry was carried at 10 mV under open-circuit conditions as the DC polarization voltage at 60 °C for 24 h. EIS was carried out in a frequency range 0.5 MHz–100 mHz with an applied voltage of 10 mV at 60 °C. The  $t_+$  value was estimated from Equation (1)

$$t_+ = \frac{I_s(\Delta V - I_0 R_0)}{I_0(\Delta V - I_s R_s)} \quad (1)$$

where  $I_0$  is the initial current,  $I_s$  is the steady-state current,  $R_0$  is the initial resistance of Li/electrolyte interface ( $R_{Li/SPE}$ ) (before the polarization),  $R_s$  is the steady-state resistance of Li/electrolyte interface ( $R_{Li/SPE}$ ) (after the polarization), and  $\Delta V$  is the applied voltage (10 mV). All plots from EIS measurements were fitted with the equivalent circuit model shown in Figure S1, Supporting Information.

#### Battery Cell Assembly

LFP and AB were dried in a vacuum at 140 °C for 2 h before use. PVDF, P(DMC), and *branch-P*(DMC/TEG/SPG) were dried in a vacuum at

110 °C for 5 h before use. For preparation of the cathode, LFP, AB, and PVDF in weight ratio 85:5:10 were dissolved in NMP in an Ar gas-filled glovebox. The materials were mixed by a planetary mixer (Thinky Co., Japan) at 2000 rpm for 20 min, then coated on Al foil using an aluminum mold (20 µm, Ø12 mm), and vacuum dried at 80 °C for 24 h. This electrode was pressed at 80 °C for 10 min and was then punched into discs (Ø16 mm). For the preparation of SPE, P(DMC) or branch-P(TEG/SPG) and LiTFSI at weight ratio 4:6 were dissolved in THF. A filter paper punched on to the O-ring (Ø16 mm for outer and Ø12 mm for inner) was set on the outside of the cathode, and the THF solution was poured on to the cathode surface. The solvent was dried at 65 °C for 8 h under normal pressure, and vacuum dried at 65 °C for 72 h. The cathode mass loading, active mass loading, cathode thickness, and the estimated electrolyte thickness of each cell are shown in Figure 4–6. The electrolyte thickness was estimated to be 260 µm minus the thickness of the cathode. Finally, a CR2032-type coin cell was assembled after putting Li metal foil on to the SPE layer (see Scheme S1, Supporting Information).

### Electrochemical Measurement

The galvanostatic charge and discharge test was carried out using a HJ-1020mSD8 (Hokuto Denko Co., Japan) at 60 °C. All cells were maintained at 60 °C for 24 h before measurements. EIS measurements for cells were conducted using an impedance analyzer VSP-300 (Bio-Logic Co., France) in the frequency range 3 MHz–100 mHz with an applied amplitude of 30 mV at 60 °C. All plots from EIS measurements were fitted using the equivalent circuit model shown in Figure S2, Supporting Information.

### Characterization of the Cathode Surface

After the 30th cycle, the battery cell was washed with THF in the glovebox and dried under vacuum at 25 °C for 24 h. The morphology of the cathode was observed by SEM using a SU3500 (Hitachi High Tech Co., Japan). The chemical composition and depth profiling of the CEI were determined by XPS using a K-Alpha (Thermo Scientific Co., USA) with monochromatized Al  $\text{K}\alpha$  (1486.7 eV) radiation. To obtain a depth profile, the topmost surface layers were removed by Ar ion-beam sputtering (200 eV) at a rate of 0.07 nm s<sup>-1</sup> (the thickness is Ta<sub>2</sub>O<sub>5</sub> equivalent).

### Acknowledgements

This work was partially supported by a Grant-in-Aid for Scientific Research (B) of JSPS KAKENHI (grant no. 23K23057).

### Conflict of Interest

The authors declare no conflict of interest.

### Data Availability Statement

The data that support the findings of this study are available in the supplementary material of this article.

**Keywords:** lithium metal batteries • polycarbonates • solid polymer electrolytes • spiroacetal rings

- [1] Y. Miao, L. Liu, Y. Zhang, Q. Tan, J. Li, *J. Hazard. Mater.* **2022**, 425, 127900.
- [2] F. Mohammadi, M. Saif, *e-Prime - Adv. Electr. Eng. Electron. Energy* **2023**, 3, 100127.
- [3] P. H. Camargos, P. H. J. dos Santos, I. R. dos Santos, G. S. Ribeiro, R. E. Caetano, *Int. J. Energy Res.* **2022**, 46, 19258.
- [4] A. G. Olabi, Q. Abbas, P. A. Shinde, M. A. Abdelkareem, *Energy* **2023**, 266, 126408.
- [5] Y. Liu, Q. Zeng, Z. Li, A. Chen, J. Guan, H. Wang, S. Wang, L. Zhang, *Adv. Sci.* **2023**, 10, 2206978.
- [6] C. Wang, J. T. Kim, C. Wang, X. Sun, *Adv. Mater.* **2023**, 35, 2209074.
- [7] L. Tang, B. Chen, Z. Zhang, C. Ma, J. Chen, Y. Huang, F. Zhang, Q. Dong, G. Xue, D. Chen, C. Hu, S. Li, Z. Liu, Y. Shen, Q. Chen, L. Chen, *Nat. Commun.* **2023**, 14, 2301.
- [8] C. Wang, X. Zhang, X. Sun, Y. Zhang, Q. Wang, J. Sun, *Macromol. Rapid Commun.* **2024**, 45, 2300645.
- [9] X. B. Cheng, R. Zhang, C. Z. Zhao, Q. Zhang, *Chem. Rev.* **2017**, 117, 10403.
- [10] Z. Wang, J. Liu, M. Wang, X. Shen, T. Qian, C. Yan, *Nanoscale Adv.* **2020**, 2, 1828.
- [11] J. F. Ding, Y. T. Zhang, R. Xu, R. Zhang, Y. Xiao, S. Zhang, C. X. Bi, C. Tang, R. Xiang, H. S. Park, Q. Zhang, J. Q. Huang, *Green Energy Environ.* **2023**, 8, 1509.
- [12] J. B. Goodenough, K. S. Park, *J. Am. Chem. Soc.* **2013**, 135, 1167.
- [13] C. Wang, C. Yang, Z. Zheng, *Adv. Sci.* **2022**, 9, 2105213.
- [14] F. Wu, Y. X. Yuan, X. B. Cheng, Y. Bai, Y. Li, C. Wu, Q. Zhang, *Energy Storage Mater.* **2018**, 15, 148.
- [15] M. Nagasaki, K. Nishikawa, K. Kanamura, *J. Electrochem. Soc.* **2019**, 166, A2618.
- [16] R. Wang, W. Cui, F. Chu, F. Wu, *J. Energy Chem.* **2020**, 48, 145.
- [17] R. Zhang, X. Shen, Y. T. Zhang, X. L. Zhong, H. T. Ju, T. X. Huang, X. Chen, J. D. Zhang, J. Q. Huang, *J. Energy Chem.* **2022**, 71, 29.
- [18] C. Arbizzani, G. Gabrielli, M. Mastragostino, *J. Power Sources* **2011**, 196, 4801.
- [19] Q. Lu, Y. B. He, Q. Yu, B. Li, Y. V. Kaneti, Y. Yao, F. Kang, Q. H. Yang, *Adv. Mater.* **2017**, 29, 1604460.
- [20] Y. Chen, Y. Zhang, J. Niu, H. Xu, Z. Dong, J. Xu, C. Lei, *ACS Appl. Energy Mater.* **2023**, 6, 3113.
- [21] X. Zhang, A. Wang, X. Liu, J. Luo, *Acc. Chem. Res.* **2019**, 52, 3223.
- [22] J. Qian, W. A. Henderson, W. Xu, P. Bhattacharya, M. Engelhard, O. Borodin, J. G. Zhang, *Nat. Commun.* **2015**, 6, 6362.
- [23] T. Yang, T. Qian, X. Shen, M. Wang, S. Liu, J. Zhong, C. Yan, F. Rosei, *J. Mater. Chem. A* **2019**, 7, 14496.
- [24] X. Hu, M. Jing, H. Yang, Q. Liu, F. Chen, W. Yuan, L. Kang, D. Li, X. Shen, *J. Colloid Interface Sci.* **2021**, 590, 50.
- [25] J. C. Barbosa, R. Gonçalves, C. M. Costa, S. Lanceros-Méndez, *ACS Omega* **2022**, 7, 14457.
- [26] L. Chen, Y. F. Huang, J. Ma, H. Ling, F. Kang, Y. B. He, *Energy Fuels* **2020**, 34, 13456.
- [27] Z. Gao, H. Sun, L. Fu, F. Ye, Y. Zhang, W. Luo, Y. Huang, *Adv. Mater.* **2018**, 30, 1705702.
- [28] S. Boulineau, M. Courty, J. M. Tarascon, V. Viallet, *Solid State Ionics* **2012**, 221, 1.
- [29] H. Wang, L. Sheng, G. Yasin, L. Wang, H. Xu, X. He, *Energy Storage Mater.* **2020**, 33, 188.
- [30] V. Bocharova, A. P. Sokolov, *Macromolecules* **2020**, 53, 4141.
- [31] D. E. Fenton, J. M. Parker, P. V. Wright, *Polymer (Guildford)* **1973**, 14, 589.
- [32] X. Y. Liu, Y. H. Chen, X. Liu, P. F. Wang, J. Shu, Z. L. Liu, Y. B. He, T. F. Yi, *J. Power Sources* **2024**, 623, 235422.
- [33] M. A. Ratner, D. F. Shriver, *Chem. Rev.* **1988**, 88, 109.
- [34] A. E. Gerdroodbar, H. Alihemmati, S. A. Safavi-Mirmahaleh, M. Golshan, R. Damircheli, S. N. Eliseeva, M. Salami-Kalajahi, *J. Energy Storage* **2023**, 74, 109311.
- [35] K. P. Barteeau, M. Wolffs, N. A. Lynd, G. H. Fredrickson, E. J. Kramer, C. J. Hawker, *Macromolecules* **2013**, 46, 8988.
- [36] S. Li, Y. M. Chen, W. Liang, Y. Shao, K. Liu, Z. Nikolov, Y. Zhu, *Joule* **2018**, 2, 1838.
- [37] Y. Zhao, L. Wang, Y. Zhou, Z. Liang, N. Tavajohi, B. Li, T. Li, *Adv. Sci.* **2021**, 8, 2003675.
- [38] C. He, H. Ying, L. Cai, H. Chen, Z. Xu, S. Liu, P. Huang, H. Zhang, W. Song, J. Zhang, L. Shi, W. Gao, D. Li, W. Han, *Adv. Funct. Mater.* **2024**, 34, 2410350.
- [39] J. Liang, D. Chen, K. Adair, Q. Sun, N. G. Holmes, Y. Zhao, Y. Sun, J. Luo, R. Li, L. Zhang, S. Zhao, S. Lu, H. Huang, X. Zhang, C. V. Singh, X. Sun, *Adv. Energy Mater.* **2021**, 11, 2002455.
- [40] X. Yang, Q. Sun, C. Zhao, X. Gao, K. R. Adair, Y. Liu, J. Luo, X. Lin, J. Liang, H. Huang, L. Zhang, R. Yang, S. Lu, R. Li, X. Sun, *Nano Energy* **2019**, 61, 567.

- [41] W. Zhou, Z. Wang, Y. Pu, Y. Li, S. Xin, X. Li, J. Chen, J. B. Goodenough, *Adv. Mater.* **2019**, *31*, 1805574.
- [42] H. Liang, L. Wang, A. Wang, Y. Song, Y. Wu, Y. Yang, X. He, *Nano-Micro Lett.* **2023**, *15*, 1.
- [43] S. J. Tan, X. X. Zeng, Q. Ma, X. W. Wu, Y. G. Guo, *Electrochem. Energy Rev.* **2018**, *1*, 113.
- [44] J. Y. Song, Y. Y. Wang, C. C. Wan, *J. Power Sources* **1999**, *77*, 183.
- [45] J. Mindemark, M. J. Lacey, T. Bowden, D. Brandell, *Prog. Polym. Sci.* **2018**, *81*, 114.
- [46] Y. Tominaga, V. Nanthana, D. Tohyama, *Polym. J.* **2012**, *44*, 1155.
- [47] Y. Tominaga, K. Yamazaki, *Chem. Commun.* **2014**, *50*, 4448.
- [48] L. Meabe, N. Lago, L. Rubatat, C. Li, A. J. Müller, H. Sardon, M. Armand, D. Mecerreyes, *Electrochim. Acta* **2017**, *237*, 259.
- [49] J. Zhang, J. Yang, T. Dong, M. Zhang, J. Chai, S. Dong, T. Wu, X. Zhou, G. Cui, *Small* **2018**, *14*, 1800821.
- [50] B. Sun, J. Mindemark, K. Edström, D. Brandell, *Solid State Ionics* **2014**, *262*, 738.
- [51] A. Flament, M. Desse, P. Bernard, C. Carrot, *Macromol. Rapid Commun.* **2024**, *45*, 2400046.
- [52] T. Morioka, K. Nakano, Y. Tominaga, *Macromol. Rapid Commun.* **2017**, *38*, 1600652.
- [53] K. Kimura, J. Motomatsu, Y. Tominaga, *J. Polym. Sci. Part B: Polym. Phys.* **2016**, *54*, 2442.
- [54] N. Soontornnon, K. Kimura, Y. Tominaga, *J. Mater. Chem. A* **2024**, *12*, 20278.
- [55] S. Ishii, N. Nishimura, Y. Tominaga, *Macromolecules* **2023**, *56*, 8878.
- [56] J. Zhang, H. Yu, X. Zhang, M. Xia, X. Zhang, L. Zhang, M. Shui, Y. Cui, J. Shu, *Ionics (Kiel)* **2021**, *27*, 31.
- [57] J. Li, Y. Ji, H. Song, S. Chen, S. Ding, B. Zhang, L. Yang, Y. Song, F. Pan, *Nano-Micro Lett.* **2022**, *14*, 191.
- [58] B. Sun, C. Xu, J. Mindemark, T. Gustafsson, K. Edström, D. Brandell, *J. Mater. Chem. A* **2015**, *3*, 13994.
- [59] S. A. Freunberger, Y. Chen, Z. Peng, J. M. Griffin, L. J. Hardwick, F. Bardé, P. Novák, P. G. Bruce, *J. Am. Chem. Soc.* **2011**, *133*, 8040.
- [60] E. G. Leggesse, R. T. Lin, T. F. Teng, C. L. Chen, J. C. Jiang, *J. Phys. Chem. A* **2013**, *117*, 7959.
- [61] Y. Tominaga, Y. Kinno, K. Kimura, *Electrochim. Acta* **2019**, *302*, 286.
- [62] X. Peng, H. Liu, Q. Yin, J. Wu, P. Chen, G. Zhang, G. Liu, C. Wu, Y. Xie, *Nat. Commun.* **2016**, *7*, 11782.
- [63] N. Soontornnon, K. Kimura, Y. Tominaga, *ACS Appl. Energy Mater.* **2024**, *7*, 4190.
- [64] F. Kaneko, S. Wada, M. Nakayama, M. Wakihara, J. Koki, S. Kuroki, *Adv. Funct. Mater.* **2009**, *19*, 918.
- [65] J. Peng, D. Lu, S. Wu, N. Yang, Y. Cui, Z. Ma, M. Liu, Y. Shi, Y. Sun, J. Niu, F. Wang, *J. Am. Chem. Soc.* **2024**, *146*, 11897.
- [66] M. Hekmatfar, A. Kazzazi, G. G. Eshetu, I. Hasa, S. Passerini, *ACS Appl. Mater. Interfaces* **2019**, *11*, 43166.
- [67] G. G. Eshetu, T. Diemant, S. Grugeon, R. J. Behm, S. Laruelle, M. Armand, S. Passerini, *ACS Appl. Mater. Interfaces* **2016**, *8*, 16087.
- [68] V. Wurster, C. Engel, H. Graebe, T. Ferber, W. Jaegermann, R. Hausbrand, *J. Electrochem. Soc.* **2019**, *166*, A5410.
- [69] C. Wang, T. Wang, L. Wang, Z. Hu, Z. Cui, J. Li, S. Dong, X. Zhou, G. Cui, *Adv. Sci.* **2019**, *6*, 1901036.
- [70] M. R. Busche, T. Drossel, T. Leichtweiss, D. A. Weber, M. Falk, M. Schneider, M. L. Reich, H. Sommer, P. Adelhelm, J. Janek, *Nat. Chem.* **2016**, *8*, 426.
- [71] S. Liu, L. Wang, C. Zhang, B. Chu, C. Wang, T. Huang, A. Yu, *J. Power Sources* **2019**, *438*, 226979.
- [72] T. Kim, L. K. Ono, Y. Qi, *J. Mater. Chem. A* **2023**, *11*, 221.
- [73] R. Dedryvère, S. Leroy, H. Martinez, F. Blanchard, D. Lemordant, D. Gonbeau, *J. Phys. Chem. B* **2006**, *110*, 12986.
- [74] H. Chen, C. J. Zhou, X. R. Dong, M. Yan, J. Y. Liang, S. Xin, X. W. Wu, Y. G. Guo, X. X. Zeng, *ACS Appl. Mater. Interfaces* **2021**, *13*, 22978.
- [75] D. Aurbach, E. Pollak, R. Elazari, G. Salitra, C. S. Kelley, J. Affinito, *J. Electrochem. Soc.* **2009**, *156*, A694.
- [76] G. G. Eshetu, X. Judez, C. Li, M. Martinez-Ibañez, I. Gracia, O. Bondarchuk, J. Carrasco, L. M. Rodriguez-Martinez, H. Zhang, M. Armand, *J. Am. Chem. Soc.* **2018**, *140*, 9921.
- [77] M. Herstedt, A. M. Andersson, H. Rensmo, H. Siegbahn, K. Edström, *Electrochim. Acta* **2004**, *49*, 4939.

Manuscript received: April 11, 2025

Revised manuscript received: June 5, 2025

Version of record online: July 9, 2025